Heat Transfer Predictions in Smooth and Ribbed Two-Pass Cooling Channels under Stationary and Rotating Conditions

Michael Göhring, Tobias Krille, Julian Feile, Jens Von Wolfersdorf

Heat Transfer Predictions in Smooth and Ribbed Two-Pass Cooling Channels under Stationary and Rotating Conditions

Michael Göhring[1]*, Tobias Krille[1], Julian Feile[1], Jens von Wolfersdorf[1]

ISROMAC 2016

International Symposium on Transport Phenomena and Dynamics of Rotating Machinery

Hawaii, Honolulu

April 10-15, 2016

Abstract

In the present study stationary and rotating smooth and ribbed two-pass cooling channels were investigated numerically. The results were compared to the experimental data from Wagner et al. [1] and Johnson et al. [2]. The simulations were performed by incorporating the commercial solver ANSYS CFX utilizing different two-equation turbulence models. In a sensitivity analysis different modifications of the widely used SST turbulence model and an explicit algebraic Reynolds stress model were tested. The SST model in combination with the reattachment modification and the curvature correction produced the best results in this study. Furthermore, the influence of the inlet boundary condition was investigated under rotation for the smooth and the ribbed configuration. Both block profiles and developed profiles with and without swirl were incorporated. The Reynolds number was 25,000 and the inlet coolant-to-wall density ratio was 0.13. For the rotation numbers 0, 0.24 and 0.36 the flow field and the heat transfer were investigated comprehensively. Both the prominent heat transfer characteristics in the first pass and the minor changes in the second pass could be reproduced in a satisfying way.

Keywords

heat transfer — rotating machinery — fluid dynamics

[1] *Institute of Aerospace Thermodynamics, University of Stuttgart, Stuttgart, Germany*

*__Corresponding author__: michael.goehring@itlr.uni-stuttgart.de

INTRODUCTION

Internal cooling channels of turbine blades are essential components of gas turbines. By increasing the turbine inlet temperature, the thermal efficiency can be augmented significantly. However, the melting temperatures of the blade materials are already exceeded by far and therefore some part of the compressed air is used to cool the blades. For an efficient cooling system the processes and dependencies of the specific cooling method have to be understood in detail. An overview of feasible internal cooling techniques is presented in various reviews, e.g. Han et al. [3] and Weigand et al. [4] .

Regarding the gas turbine rotor blade, the effects of rotation are inevitable and have to be considered. For rotating ribbed multi-pass cooling channels a pioneer work has been done by Wagner et al. [1] and Johnson et al. [2]. They accounted for the effects of rotation in terms of Coriolis and centrifugal forces and determined segmental area averaged Nusselt numbers. Thorough parameter studies were done by varying the Reynolds number, the rotation number and the centrifugal buoyancy, following the dimensions of real engine applications. The published works were supported by the NASA/Lewis Research Center. This is why in the following they will be referred to as the investigations on the NASA channel.

A vast number of experimental and numerical works on internal cooling channels has been published during the last decades. Often, the results by Wagner et al. [1] and Johnson et al. [2] have been taken as reference data. Geometrically different channel forms have been investigated, varying in the number of passes, the kind of turbulence promotors and the cross-section area. Within the numerical works, not only Reynolds avaraged Navier-Stokes (RANS) and unsteady RANS (URANS) approaches were employed (and thus different turbulence models) but also Detached Eddy Simulations (DES) and Large Eddy Simulations (LES).

The works by Prakash and Zerkle [5] and Tolpadi [6] are among the first publications in which numerical results were compared to the NASA channel. Both studied rotating smooth rectangular passes with the $k-\varepsilon$ turbulence model and posted that the three main unknown are the uncertainty in the experimental data, the specifications of inlet conditions and the ability of the turbulence modeling to account for rotation and buoyancy effects. Similar findings are shown in Iacovides et al. [7]. Bo et al. [8] also investigated a smooth one-pass cooling channel by utilizing different turbulence models. Good results were found with the $k-\varepsilon$ turbulence model as well as with a low-Re algebraic Reynolds stress model (ASM) that accounts for the anisotropy of the turbulence. Bonhoff et al. [9, 10] predicted the heat transfer in smooth and ribbed two-pass cooling channels that were similarly shaped as the ducts of the NASA channel. They investigated the influence of turbulence models and rotation on the heat transfer. With their simulations they gave a first detailed insight into the flow field and the heat transfer of two-pass cooling channels. For their studies they used the commercial CFD-code FLUENT.

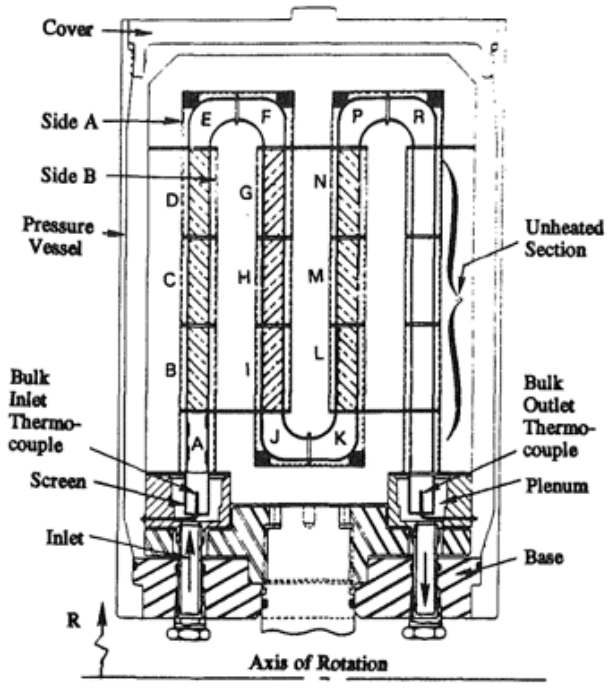

Figure 1. Four-pass cooling channel by Johnson et al. [2]

Other comparisons to the experimental NASA channel results were conducted by Chen et al. [11] and Jang et al. [12] using the chimera RANS method. Jang et al. simulated a rotating single-pass cooling channel with and without ribs at a Reynolds number of 25,000. They incorporated a Reynolds stress turbulence model (RSM) and compared the results for three rotation numbers ($Ro = 0; 0.13; 0.24$) and one density ratio ($\Delta\rho/\rho = 0.13$). Chen et al. investigated a smooth two-pass cooling channel and compared the two-layer $k-\varepsilon$ model with the RSM results. They made calculations for different rotation numbers ($Ro = 0; 0.118; 0.24$) and density ratios ($\Delta\rho/\rho = 0.07; 0.13; 0.22$). In both publications it is said that the development of momentum and thermal boundary layers is significantly influenced by the Coriolis and buoyancy forces that produce strong nonisotropic turbulence. They state that it is therefore important to employ second-order moment closure models. Another non-commercial CFD-code was employed by Lin et al. [13] using CFL3D. In this publication a U-duct with some ribs close to the bend was simulated. Results were compared to a smooth channel with a Reynolds number of 25,000, a rotation number of 0 and 0.24 and a density ratio of 0.13. With this set of parameters and the $k-\omega$ SST turbulence model they showed good agreement to the experimental NASA data. In Stephens and Shih [14] similar parameters were varied for the smooth case of the investigated U-duct. They also showed good agreement with the incorporated SST turbulence model. Nikas and Iacovides [15] studied smooth two-pass square-ended U-bends with numerical methods. Their parameters included Reynolds numbers of 36,000 and 100,000 under rotating conditions ($Ro = 0.2$). For the simulations they used the CFD-code STREAM and tested several turbulence models. Even with their simplest turbulence model (a two-layer $k-\varepsilon$ model) the mean flow development was within reasonable accuracy. The low-Re models showed to be superior to the two-layer models and finally differential stress models in the low-Re formulation showed the best agreement with the experimental data.

Lately, more computationally intensive appraoches have been incorporated for the simulation of cooling channels. URANS (compare Saha and Acharya [16]), DES (compare Viswanathan and Tafti [17]) and LES (compare Murata and Mochizuki [18]) were performed. However, limitations of geometrical complexity and operating conditions (at high Reynolds numbers) have to be accepted if the computer capacities are confinded.

The present study is a numerical investigation on smooth and ribbed two-pass cooling channels that are very close to the geometry used by Wagner et al. and Johnson et al. (compare section 1.1). We employ RANS simulations in combination with two-equation turbulence models and are therefore capable of simulating various operating conditions. The aim of this investiagtion is to validate the numerical results performed with the commercial CFD-code ANSYS CFX 15.0. Within this study we discuss the sensitivity of turbulence modeling and investigate the effect of different inlet boundary conditions. The heat transfer is evaluated for three different rotation numbers.

1. NUMERICAL METHOD

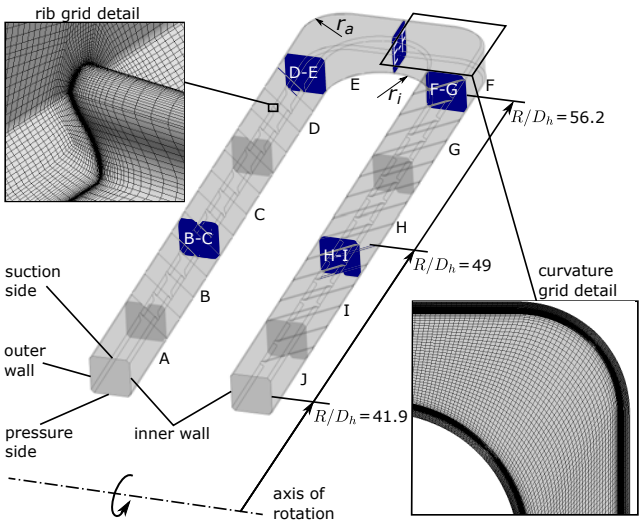

Figure 2. Modeled two-pass cooling channel with two numerical grid detail views

The computational fluid dynamics are performed with the finite-volume solver ANSYS CFX 15.0, which is a fully implicit, coupled multigrid solver. For the stationary solution of the problem the Reynolds averaged Navier-Stokes equations are utilised. The closure problem is undertaken by using the SST turbulence model with different modifications and features that are available in CFX (see section 3). For all

cross section	R/D_h
E-F (middle)	57.9
D-E / F-G	56.2
C-D / G-H	52.3
B-C / H-I	48.5
A-B / I-J	44.6
A_{in} / J_{out}	41.9

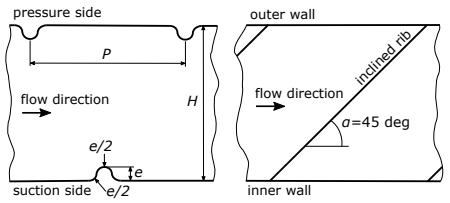

Figure 3. Local rotation radii and details on staggered rib arrangement

computations the default quasi-second order discretization scheme in CFX, called High Resolution, is applied.

Air is modeled as ideal gas and is therefore regarded as compressible fluid. Both the viscosity and the thermal conductivity change with temperature (Sutherlands formula, see e.g. White [19]).

The inlet Reynolds number is $Re_{in} = (\rho_{in} v_{b,in} D_h)/\eta_{in} = (\dot{m} D_h)/(A\eta_{in}) = 25,000$ according to a massflow of $\dot{m} = 0.0059\,\mathrm{kg/s}$ and an inlet temperature of $T_{in} = 26.67\,^{\circ}\mathrm{C}$. The wall temperature is $T_{wall} = 71.11\,^{\circ}\mathrm{C}$ which yields an inlet-to-wall density ratio of $\Delta\rho/\rho = (\rho_{in} - \rho_{Wall})/\rho_{in} = 0.13$. For the three different rotation numbers $Ro = (\Omega D_h)/v_{b,in} = (\Omega D_h \rho_{in} A)/\dot{m} = \{0; 0.24; 0.36\}$ rotational speeds of 0 rpm, 550 rpm and 825 rpm are applied.

1.1 Geometry

The investigated geometry is shown in Figure 2. The two-pass cooling channel is a reproduced geometry of the experimental studies from Wagner et al. [1] and Johnson et al. [2]. In this study only the first two of four legs are simulated that are connected by a 180° bend. The cross-section area of the straight parts is square with a side length of $H = 12.7\,\mathrm{mm}$. However, due to the experimental procedure, there are chamfer of 1.0 mm in each corner that provide an isolation of the copper elements. This is included in the numerical domain. The hydraulic diameter in the straight sections therefore becomes $D_h = 13.2\,\mathrm{mm}$. The channel walls are heated to a constant temperature, except the inner wall of the bend. The heated length of the first passage is 14.3 hydraulic diameters and consisted in the experiment out of 16 copper elements that were also isolated in the streamwise direction (not included in this study). The inner bend radius is $r_i = 1.25H$, the outer radius is $r_a = H$. In the rotating case the mean rotation radius is equal to the default experimental mean radius of $\bar{R}/D_h = 49$. The local rotation radii are listed in Figure 3. Inside the ribbed configuration there are circular shaped ribs on the pressure and suction surfaces of the straight passes (segments B to D and G to I). They are arranged in a staggered layout as indicated in Figure 3. The rib turbulators are inclined towards the mean flow direction by $\alpha = 45\,\mathrm{deg}$. The rib height ratio is $e/H = 1/10$ and the pitch to rib height ratio is $P/e = 10$.

In thr ribbed case each copper segment has a length of $4H$ and therefore includes 4 ribs. As the blocking of the computational mesh yields a constant dimensionless wall distance (see section 1.2), the half ribs from cross sections D-E and F-G (compare Figure 1) are moved towards cross sections A-B and I-J, respectively. As depicted in Figure 2 the ribs are in contact to the inner and outer walls.

The channel has been extended by smooth adiabatic sections at the inlet and outlet (with a typical copper segment length of $4H$, not shown in Figure 2). By this, the development of the flow field and the thermal boundary layer shall be considered similarly to the experiment (compare inflow section in Figure 1).

1.2 Grid generation

The multi-block structured grids have been generated with ANSYS ICEM CFD 15.0. Some details of the computational grids are included in Figure 2. To better control the dimensionless wall distance and the growth ratio close to the wall several cuts have been integrated. For a sensible spatial resolution of the ribs O-grids have been employed. This can fairly be done for complete ribs but would be quite complex for half ribs. The challenge would be a proper blocking along the rib in the region of the cut. Additional O-grids and blocks could be imposed but would tend to a very extensive blocking, particularly if the dimensionless wall distance has to be restricted. That is why half ribs were eliminated in this study (see section 1.1).

The assessment of the grid independence is valued by a grid convergence index (GCI) study in section 2. The grids of the smooth and the ribbed two-pass cooling channels have 7 and 18 million grid points, respectively. This difference is accounted to the streamwise resolution of the ribs. The grid point numbers referred to in section 2 contain the experimental copper segments A-J only. For the evaluation of the heat transfer the dimensionless wall distance has to be restricted. In all grids it has been verified that the dimensionless wall distance of the first node satisfies $y^+ \approx 1$. All grid quality parameters like grid angle, aspect ratio and volume change are within the ranges prescribed by the CFX-Manual [20].

1.3 Data evaluation

In the experimental data analysis the Nusselt number and the Reynolds number were evaluated for each copper segment. The reference temperature for the heat transfer coefficient was calculated to be the arithmetic mean value of the incoming and outgoing bulk temperatures of a copper segment. These bulk temperatures were calculated with a thermodynamic energy balance over each channel segment knowing only the temperature at the inlet (measured with a thermocouple). The fluid properties in the Nusselt number and Reynolds number were calculated at the film temperature (which is defined as the mean value of the reference and the wall temperature). Finally, the Nusselt number was referred to a correlation for the turbulent flow in a smooth tube after Kays and Perkins [21] with a Prandtl number of 0.72: $Nu_\infty = 0.0176\, Re^{0.8}$.

This procedure has been conducted for the numerical results in equal measure. However, the bulk temperatures at the inlet and outlet of a segment were determined from the computational results. Additionally, we comprised a refined

data evaluation by averaging the heat transfer results within a rib segment instead of a copper segment (channel length of $H = 12.7$ mm instead of $4H$).

The segment nomenclature follows Figure 2. The first pass includes segments A to D, the bend region consists of segments E and F, the second pass contains segments G to J. Segment J is different compared to the experiment, where it was part of the bend. The data evaluation is hence only performed for segments A to I. In the following, the abbreviations PS (pressure side), SS (suction side), OW (outer wall) and IW (inner wall) are used.

To specify the deviation of the numerical data from the experimental results absolute values are presented. These values are also averaged over the single passes and the complete channel. In this case arithmetic mean values of the absolute values are shown. The calculated values are always evaluated for the copper segments (and not rib segments) as in the experiment, although finer evaluated data may be depicted in the diagrams.

2. GRID INDEPENDENCE STUDY

The spatial discretization error is estimated by utilizing the GCI (grid convergence index) method which is based upon a grid refinement error estimator derived from the theory of generalized Richardson extrapolation. The applied procedure follows Roache et al. [22] and Celik et al. [23]. To determine the GCI values simulations with three different grids were performed for the smooth and ribbed channel, respectively. Representative results of the pressure side are shown in Figure 4.

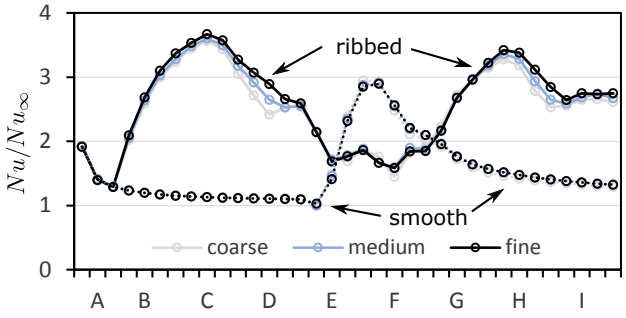

Figure 4. Heat transfer results on differently fine meshes of smooth and ribbed channels, pressure side

The biggest difference of the Nusselt number ratio in the ribbed channel can be found at the end of pass 1 (coarse grid: 2.42, fine grid: 2.89). However, at most positions in the duct the values are very similar. The differences in the smooth channel are even smaller: maximum difference inside the bend (segment F, difference: 0.17).

The evaluation of the GCI values is generally as follows (for more details, see Celik et al. [23]): taking the differences of the results and a grid refinement factor into account, the so-called apparent order can be calculated. Thereupon, extrapolated values and approximate relative errors are determined which yield the final GCI value. The GCI herein is determined for the finest meshes, respectively. A summary of the results is presented in Table 1.

The GCI values for the Nusselt number ratios of the ribbed channel are between 0 % and 124.89 % (OW, segment D, not shown). The large GCI values, however, arise from the very small differences of the coarse/medium and the medium/fine values (examplarily for the highest GCI: −0.075 and −0.072).

The grid convergence study is therefore expanded. As an overall measure of grid convergence, an average value of the apparent order as proposed by Celik et al. [23] is determined. With this, the GCIs are again evaluated, resulting in values on all walls of the ribbed channel below 5 %. In Table 1 these values are listed under 'global apparent order'. The GCI for the pressure loss in the smooth channel and the ribbed channel are 0.17 % and 13.27 % (large value due to the same reason as described above), respectively.

Table 1. Results of the grid convergence index study for the finest meshes

	smooth	ribbed
million grid cells	(5.8 , 2.9, 1.4)	(17.2, 8.2, 4.0)
Nu/Nu_∞		
local GCI	0-58.23%	0.03-124.89%
global GCI	2.23%	12.6%
Nu/Nu_∞, global apparent order		
local GCI	0-0.56%	0.1-4.92%
global GCI	0.15%	1.58%
Δp		
global GCI	0.17%	13.27%

The GCI has been conducted with the SST turbulence model in conjunction with the modifications that proved to be best in the study later on (compare section 3). Only the non-rotating conditions have been tested here. It is assumed that similar grid dependent results are established under the remaining parameter sets. In fact, it has been checked, that the dimensionless wall distance y^+ of the nearest grid point to the wall is about 1, also when rotation is applied. The here presented finest meshes are used in the further simulations.

3. SENSITIVITY STUDY ON TURBULENCE MODELING

To evaluate the influence of the turbulence model on the heat transfer results four different setups of turbulence models have been employed. Due to its stability and universal applicability, the shear stress transport model (SST) by Menter [24] has been chosen as basic model. Despite its known drawbacks, it showed to be useful in many engineering applications (as mentioned in the Introduction). However, modifications are available to overcome some of these deficiencies. Because of its known disadvantage of predicting the reattachment point in

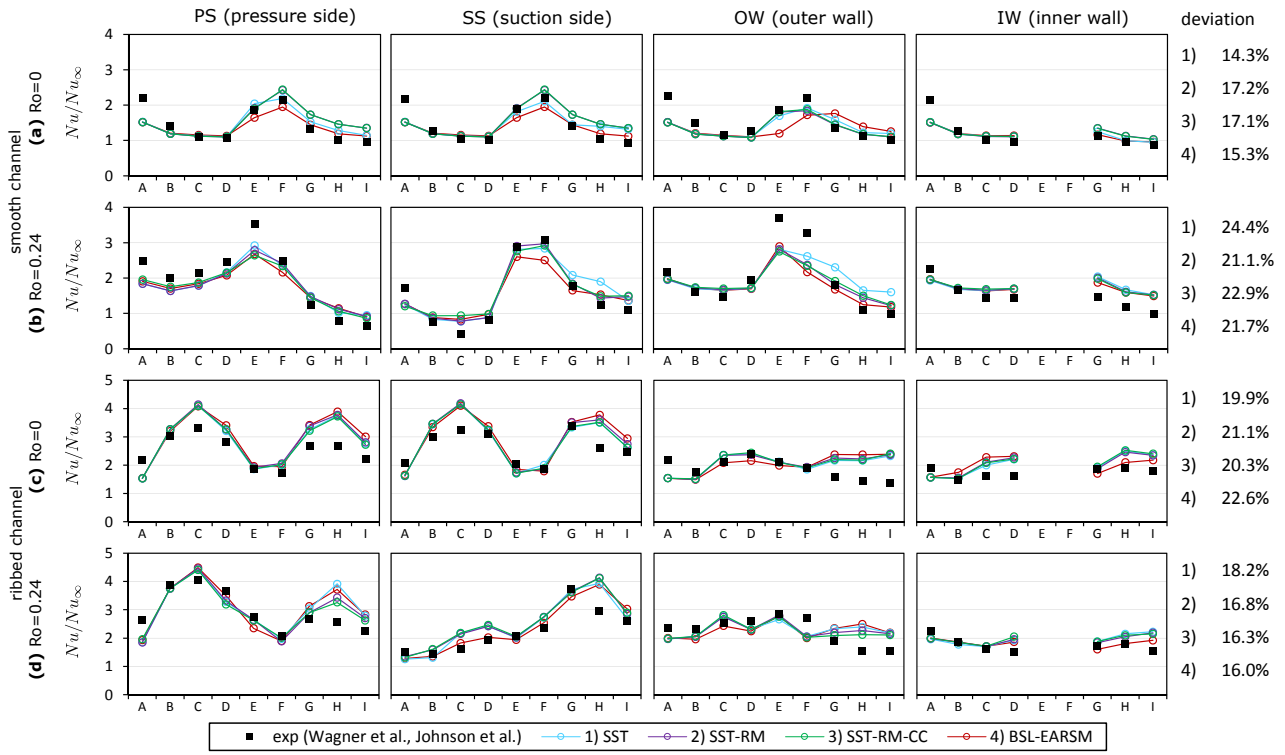

Figure 5. Heat transfer results of different turbulence models in comparison to experimental data

recirculation zones too late, the so-called reattachment modification (RM) [20] can be enabled. For rotational effects and streamline curvature the curvature correction (CC) described in Smirnov and Menter [25] can be used.

In addition, an explicit algebraic Reynolds stress model (EARSM) by Menter et al. [26] is employed. It is a further development of the two-equation models and has proven to enhance accuracy. The used EARSM in CFX incorporates the underlying BSL formulation (blending between $k-\varepsilon$ and $k-\omega$). Although it is not as accurate as differential Reynolds stress models (RSM), it incorporates the anisotropy of the Reynolds stresses and captures the effects of rotation. Differential RSM, however, suffer from stability problems and the computational costs are considerable.

As a result, we decided to present the simulation results of the following turbulence model configurations: 1) SST, 2) SST-RM, 3) SST-RM-CC, 4) BSL-EARSM. They will be judged by the quality of convergence as well as by the capability to predict the heat transfer. The study incorporates on the one side the smooth and ribbed channels, on the other side both the stationary and the rotating case ($Ro = 0.24$).

Figure 5 presents the results for all configurations on all channel walls. On the right, mean values of the deviations (averaged over PS, SS, OW, IW) are listed for the single turbulence models. The standard SST turbulence model exhibits already in the smooth non-rotating case a huge deficiency. In the second pass no symmetric heat transfer characteristic between pressure and suction side is accomplished, as would be expected (compare Figure 5a segments H and I, blue line).

This insufficiency can be cleared out by applying the reattachment modification (SST-RM). Expanding the model further by the curvature correction (SST-RM-CC) leads to smaller differences in comparison to the experimental data for most configurations (compare deviations in Figure 5, exception: b, rotating smooth channel).

With the SST-RM-CC the biggest relative deviations from the experimental results can be found in the rotating smooth channel (Figure 5b SS, segment C: 121%) and in the non-rotating ribbed channel (Figure 5c OW, segment I: 74%). The results can so far be summed up by regarding the averaged relative deviations of the SST-RM-CC turbulence model. In the smooth channel the results deviate by 17% (non-rotating) to 23% (rotating), in the ribbed channel the global deviations lie between 20% (non-rotating) and 16% (rotating). Considering the experimental uncertainty of up to 10% for the regarded cases and the simplifications that were made in this study (espeially the substitution of the second bend by a straight channel), the results can be considered acceptable.

The BSL-EARSM shows overall slightly better agreement with the experimental data in the smooth channel (overall relative deviation: 19%, SST-RM-CC 20%). In the ribbed channel the results of the BSL-EARSM are worse than those of the SST-RM-CC model (19% vs. 18%).

Considering stability and convergence behaviour, the non-rotating simulations incorporating the SST model reach maximum residuals of order 10^{-5} and 10^{-3} (smooth and ribbed channel). Under rotation the residuals for the standard SST model rise considerably (10^{-2}). In the smooth channel RM

and CC have positive influence on the stabiliy and bring the residuals down to 10^{-4}. For the ribbed channel at least sligthly better convergence can be achieved with the modifications when the channel is rotating. Using the BSL-EARSM residuals go up to 10^{-2} for the non-rotating case and are of order 10^{-1} under rotation. Taking the predictions and the convergence behaviour into account, we chose the SST-RM-CC model setup to perform the further simulations in this study.

In the following the results are limited to the evaluation of the pressure are suction sides as the effects on the heat transfer are predominant there.

The most systematic deviation from the experiment can be found in the inlet section (segment A). This disagreement has already been discussed in previous works (e.g. Prakash and Zerkle [5] and Tolpadi [6]). Within this study the heat transfer is consistently underpredicted by 15% to 25%. That is why different inlet boundary condition will be investigated in the next section.

4. SENSITIVITY STUDY ON INLET BOUNDARY CONDITION

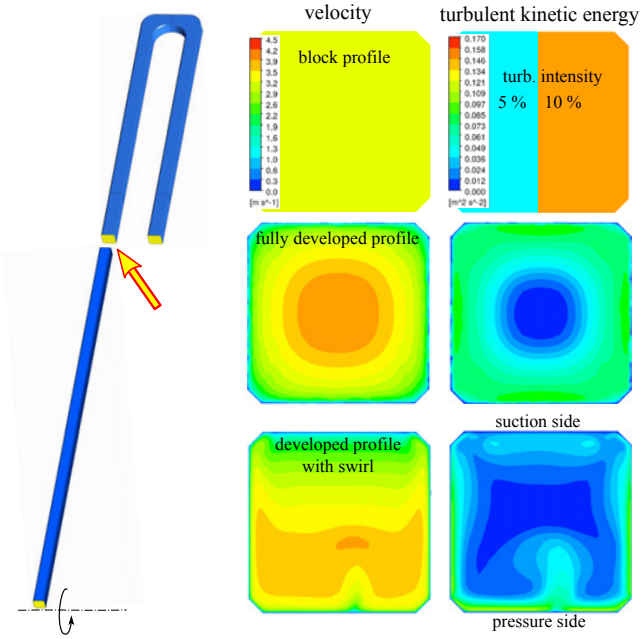

Figure 6. Different inlet boundary conditions

As depicted in section 3, the heat transfer characteristic in the inlet section was underpredicted in all cases. This underprediction was also seen in the numerical predictions of Chen et al. [11] and at least partly in Bonhoff et al. [10]. Yet, the inlet boundary condition of the experiments is not known in detail. Wagner et al. [27] stated that the centerline turbulence level was about 4%, but the flow field was not completely uniform and slightly skewed. In general, it was however supposed to be a fully developed profile.

For the simulations such a fully developed turbulent profile was provided as inlet boundary condition so far (turbulence intensity of 5.7 %). Now, we additionally examine inlet boundary conditions with block profiles of 5 % and 10 % turbulence intensity. Furthermore, a developed swirled profile (turbulence intensity of 4.0%) is included in the test. According to this, the study is performed for the rotating case.

The developed profiles have been generated with preceding simulations. For the fully developed profile an adiabatic, straight, smooth duct with the same cross section as the cooling channel itself was employed. A block profile with a turbulence intensity of 5% was set as inlet boundary condition. The later used profile was then taken from the outlet. For the swirled profile the same duct was utilized but with the fully developed profile as inlet boundary condition. This time the duct was rotated (550 rpm, according to $Ro = 0.24$) in such a way that the inlet was positioned on the axis of rotation. The outlet was placed on a radius according to the inlet radius of the cooling channel.

The profiles are shown in Figure 6. While the block profiles are uniform, typical contours are generated within both developed profiles. These seem to be reasonable, as Hwang and Jen [28] as well as Prakash and Zerkle [5] predicted similar forms. The fully developed profile is symmetric with maximum values in the middle of the channel, the main flow in the swirled profile is pushed towards the pressure side.

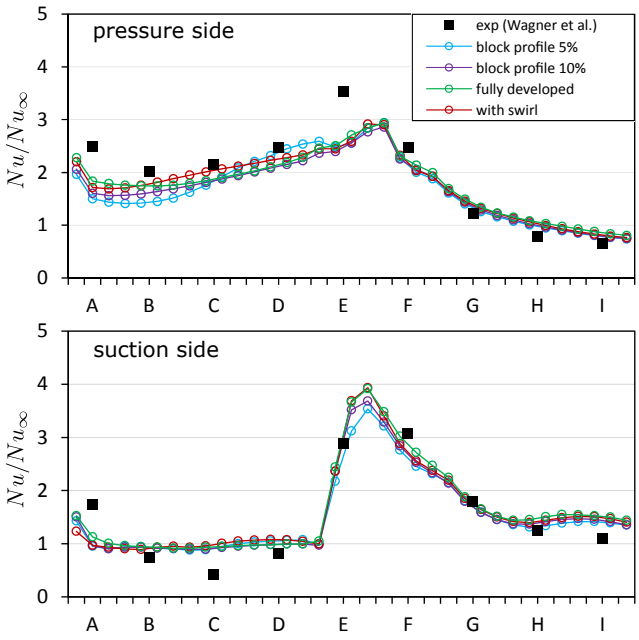

Figure 7. Nusselt number ratios for different inlet boundary conditions in the rotating smooth channel ($Ro = 0.24$)

The effect on the Nusselt number ratios is presented in Figures 7 and 8. The most prominent differences in the smooth channel can be found in segments A and B of the pressure side as well as in the bend region of the suction side. In the ribbed channel the distinctions spread over the whole channel. Additionally to the observations in the smooth channel, both developed profiles show noticable deviations from the block profiles. The swirled profile strongly deviates from the other

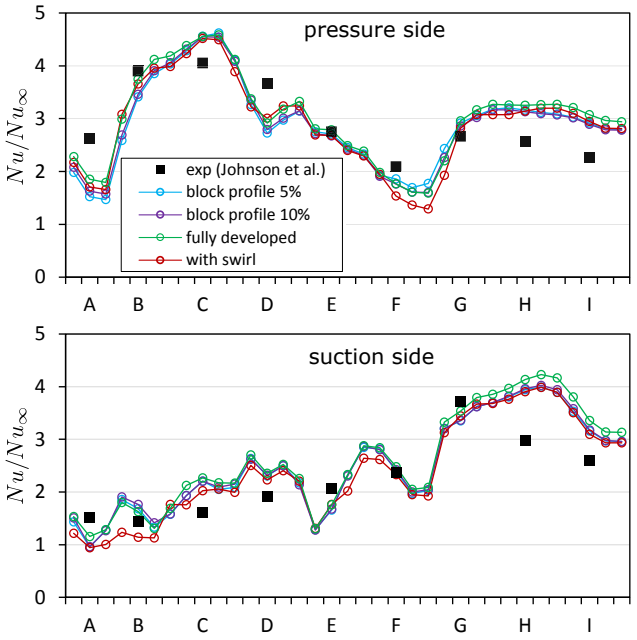

Figure 8. Nusselt number ratios for different inlet boundary conditions in the rotating ribbed channel ($Ro = 0.24$)

numerical results close to the inlet (SS) as well as in the bend region (segment E on SS, segment F on PS). Furthermore, the fully developed profile predicts higher heat transfer values in the second pass.

The relative deviations from the experimental data for segment A are presented in Table 2.

Table 2. Comparison of inlet boundary conditions, relative deviations from experimental data, segment A, values in %

boundary	smooth		ribbed	
condition	PS	SS	PS	SS
5%	34.9	37.0	37.1	37.0
10%	30.4	35.6	33.2	35.6
fully dev.	21.4	30.0	25.0	30.0
with swirl	25.3	39.8	30.0	39.8

The highest underpredictions in comparison to the experiment are generated with the block profiles: although the 10% turbulence intensity profile is closer, both block profiles are clearly more than 30% away from the experimental data. In comparison, the developed profile with swirl is closer to the experiment on the pressure side (25.3% and 30%), but underpredicts the heat transfer in segment A of the suctions sides in both the smooth and the ribbed channel more distinctly (each 39.8%). The fully developed profile is continuously closest to the experiment on all evaluated surfaces of segment A with relative deviations between 21.4% and 30%.

The strong underprediction of the heat transfer in the inlet section could not be overcome with the investigated profiles. As the fully developed profile provides the best heat transfer results in the comparison, we continue our simulations with this inlet boundary condition.

5. INFLUENCE OF ROTATION

The influence of rotation on the heat transfer is investigated for the three rotation numbers $Ro = \{0; 0.24; 0.36\}$. The flow field in terms of normalized velocity and secondary flow vectors is presentend in Figure 9. The cross sections are located in the first pass (B-C, D-E), inside the bend (E-F) and in the second pass (F-G, H-I). This is also illustrated in Figure 2. Additionally, Nusselt number ratios are presented as contour plots for selected heat transfer surfaces (on the right).

In the stationary smooth channel the flow field is very symmetric showing typical Dean type vortices inside the bend (E-F). Due to the Coriolis force (present under rotation) the fluid is clearly pushed towards the pressure side in the first pass (B-C, D-E). Thus the fluid close to the pressure side is cooler than that near the suction side. This again implicates a higher fluid density close to the pressure side. For this reason the high fluid velocities at the pressure side can be explained with the rotational buoyancy which accelerates the cool fluid and decelerates the hot fluid. This enhanced forced convection is connected to a higher heat transfer on the pressure side of the first pass and diminished Nusselt number ratios on the suction side (compare plots in Figure 9). As a result of the bend influence the reversed behaviour in the second pass (fluid flow towards suction side) is less distinct. Nevertheless, the presented heat transfer distribution matches the expectations, as the Nusselt number ratios are higher on the suction side than those on the pressure side.

In contrast to the smooth channel, the stationary ribbed channel is governed by the rib induced secondary flow that is supplemented by Dean vortices in the bend region. Again, the appearance of the Coriolis force in the rotating case is evident. Because of the highly threedimensional flow field (rib induced secondary flow, recirculation zones) complex secondary structures are formed through the whole cooling channel. On the whole, the results of the secondary flow structures are very similar to those obtained by Chen et al. [11] and Bonhoff et al. [9, 10]. The plots of the Nusselt number ratio in the ribbed channel reveal the same behaviour as in the smooth configuration. The heat transfer on the pressure side of the first pass is enhanced, the heat transfer on the suction side of the first pass is diminished.

Figures 10 and 11 present the segmental averaged Nusselt number ratios. They are supplemented by averaged deviations from the experimental data in Table 3. As described before, the heat transfer on the pressure side of the first pass rises under rotating conditions. While the smooth channel values for $Ro = 0.24$ are met quite well (15.1% deviation), the Nusselt number ratios at $Ro = 0.36$ are noticeably underpredicted (22.8%). We assume that the inlet boundary condition is in part responsible for this (highest deviations in segments A and B). On the suction side the experimental Nusselt number ratios first decrease from $Ro = 0$ to $Ro = 0.24$ and increase again for $Ro = 0.36$. This trend is also captured with the simulations, although the relative deviations are quite high.

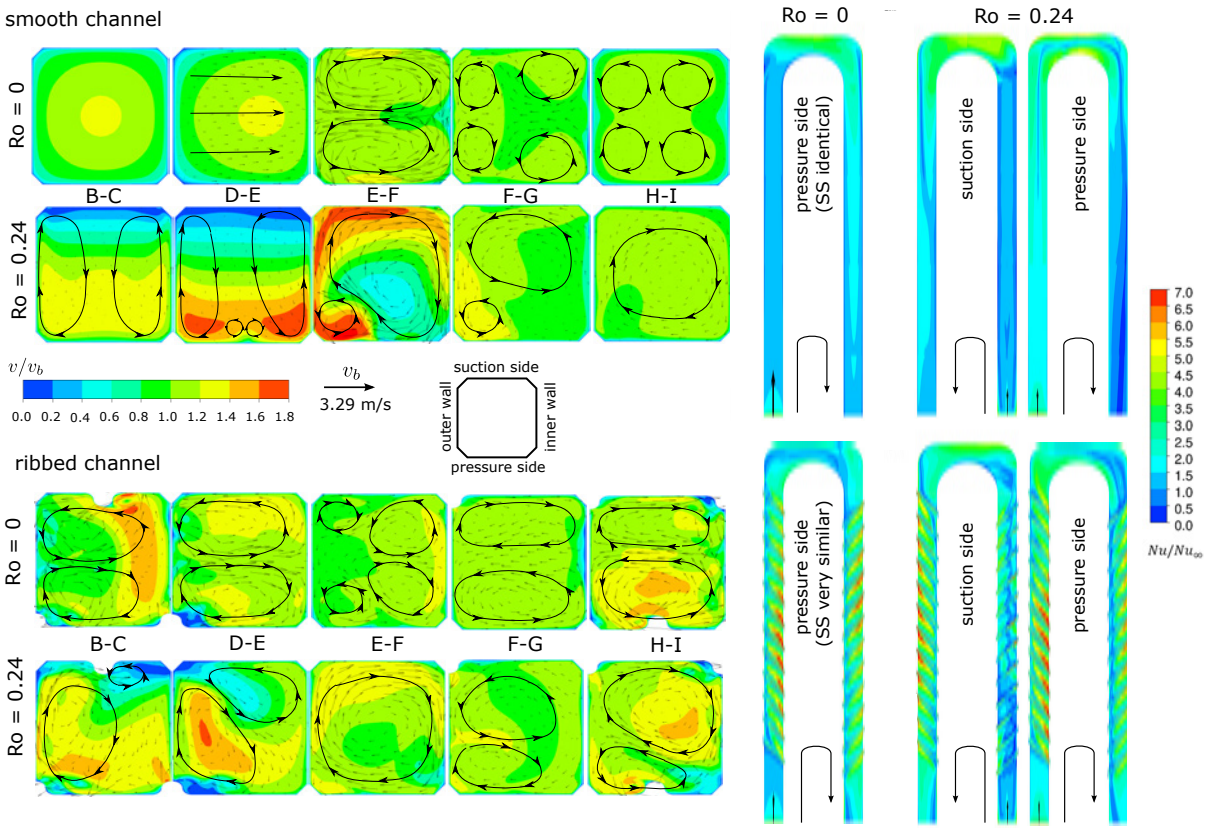

Figure 9. Influence of rotation on flow field and Nusselt number ratios in the smooth and ribbed channels

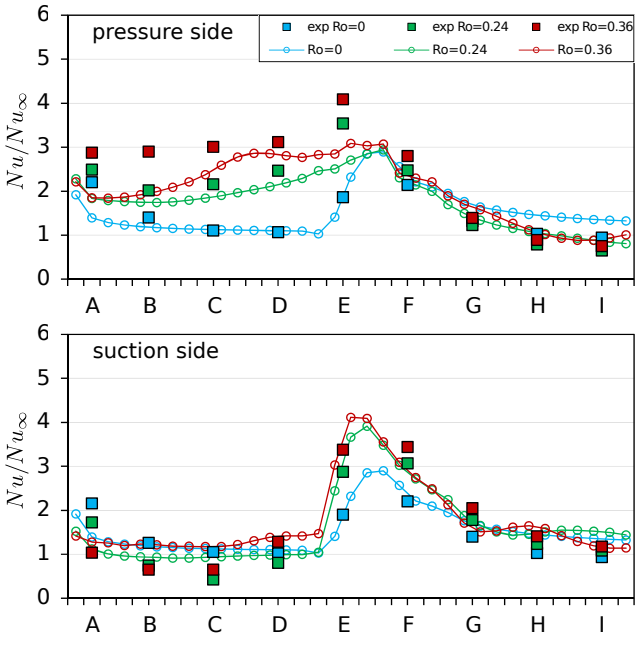

Figure 10. Influence of rotation on Nusselt number ratio for smooth channel

Due to the influence of the bend, the Nusselt number ratios in the second pass of the smooth channel do not alter as much as in the first pass. This was shown with the experiment and can be revealed with the simulations.

In the ribbed channel the trends of rising heat transfer on the pressure side of the first pass are also met quite well (deviations of 17.3%(Ro = 0), 13.5%(Ro = 0.24), 12.6%(Ro = 0.36)). On the suction side of the first pass the decrease from stationary to rotating conditions is captured properly (Figure 11) and the relative deviations are reasonably low (20.2%(Ro = 0.24), 7.4%(Ro = 0.36)). The dependency of the heat transfer on rotation in the second pass is less significant, in the simulation as well as in the experiment (see Figure 11).

In the bend region rotation generally leads to higher Nusselt number ratios. This is in good agreement with the experimental trends and the relative deviations support this (mostly below 10%). Altogether, it seems as if the trends in the smooth and in the ribbed channel match the expectations from the experiment well (compare Figures 10 and 11). However, the level of the Nusselt number ratios (Table 3) in the smooth channel is lower and the relative deviations are thus generally higher there. Averaging over all presented (PS and SS) surfaces in each configuration (all three rotation numbers) the heat transfer predictions of the smooth channel deviate from the experimental data by 23.0% and by 13.1% in the ribbed channel.

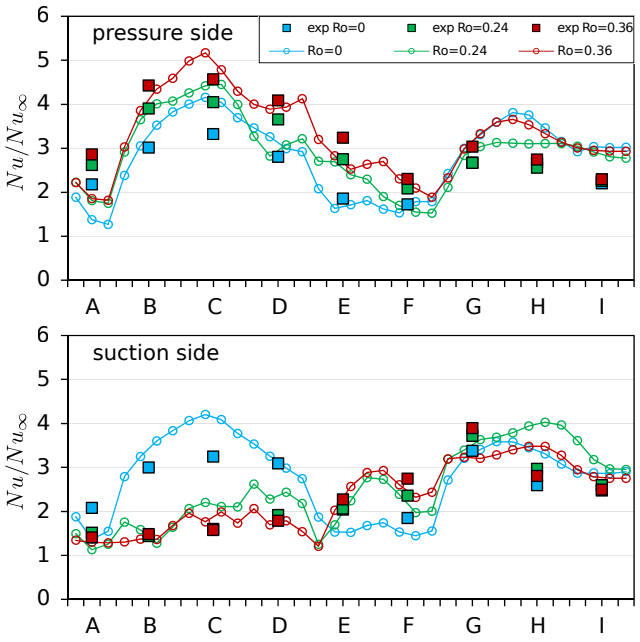

Figure 11. Influence of rotation on Nusselt number ratio for ribbed channel

Table 3. Comparison of results under rotation, relative deviation from experimental data

	pressure side			suction side		
Ro	pass1	bend	pass2	pass1	bend	pass2
smooth (values in %)						
0	12.7	7.9	38.5	12.6	5.3	36.4
0.24	15.1	15.4	28.1	49.6	4.3	20.4
0.36	22.8	19.3	21.0	50.7	9.9	9.5
ribbed (values in %)						
0	17.3	7.8	21.7	15.4	10.4	11.2
0.24	13.5	7.8	11.8	20.2	7.7	14.8
0.36	12.6	13.3	11.9	7.4	6.7	13.8

6. CONCLUSION

In the present study internal two-pass cooling channels with and without ribs were simulated with the commercial CFD-code ANSYS CFX. The modeled channels were very close to the geometry from the experiments conducted by Wagner et al. [1] and Johnson et al. [2]. The grid convergence study showed only little grid dependence. The SST turbulence model in combination with the reattachment modification and the curvature correction showed the best results in comparison to the other tested model configurations. It was capable to predict the experimental heat transfer results within an overall deviation of 19%. As the experimental inlet boundary condition was not known completely, it was modeled with different elementary assumptions. The experimental data were best met with a fully developed profile, although the deviations were still considerable (of order 25%). Finally, the flow field and the heat transfer were investigated under the three rotation numbers 0, 0.24 and 0.36. The overall averaged relative deviations from the experimental data of the Nusselt number ratios were 23% for the smooth and 13% for the ribbed cooling channel with locally higher values.

ACKNOWLEDGMENTS

The investigations were conducted as part of the joint research programme COORETEC-turbo (AG Turbo 2020) in the frame of AG Turbo. The work was supported by the Bundesministerium für Wirtschaft und Energie (BMWi) as per resolution of the German Federal Parliament under grant number 03ET2013D. The authors gratefully acknowledge AG Turbo, ALSTOM Power and MTU Aero Engines for their support and permission to publish this paper. The responsibility for the content lies solely with its authors.

NOMENCLATURE

A	m^2	cross-section area
D_h	m	hydraulic diameter
e	m	rib height
h	$W\,m^{-2}\,K^{-1}$	heat transfer coefficient
H	m	channel side length
k	$W\,m^{-1}\,K^{-1}$	thermal conductivity
$\dot{m}$	$kg\,s^{-1}$	mass flow
Nu	-	Nusselt number $(hD_h)/k$
Nu_∞	-	Nusselt number (correlation)
P	m	rib spacing pitch
R	m	rotation radius
Re	-	Reynolds number $(\rho v D_h)/\eta$
r_i, r_a	m	inner and outer bend radius
Ro	-	rotation number $(\Omega D_h)/v_{b,in}$
T	°C	temperature
v	$m\,s^{-1}$	velocity
y^+	-	dimensionless wall distance
α	deg	rib inclination angle
η	$kg\,m^{-1}\,s^{-1}$	dynamic viscosity
k, ε, ω		turbulent magnitudes
Ω	$rad\,s^{-1}$	angular velocity
Δp	Pa	pressure loss
$\Delta\rho/\rho$	-	density ratio $(\rho_{in} - \rho_{Wall})/\rho_{in}$
b	subscript	bulk value
film	subscript	value at film temperature
in	subscript	value at the inlet
wall	subscript	value at the wall
A-J		segment numbers
GCI		grid convergence index
IW, OW		inner wall and outer wall
PS, SS		pressure side and suction side
RM, CC		model modifications
SST, (EA)RSM		turbulence models

REFERENCES

[1] J. H. Wagner, B. V. Johnson, and F. C. Kopper. Heat transfer in rotating serpentine passages with smooth walls. *Journal of Turbomachinery*, 113:321–330, 1991.

[2] B. V. Johnson, J. H. Wagner, G. D. Steuber, and F. C. Yeh. Heat transfer in rotating serpentine passages with trips skewed to the flow. *Journal of Turbomachinery*, 116:113–123, 1994.

[3] J.-C. Han, S. Dutta, and S. Ekkad. *Gas Turbine Heat Transfer and Cooling Technology*. Taylor & Francis, 2000.

[4] B. Weigand, K. Semmler, and J. von Wolfersdorf. Heat transfer technology for internal passages of air-cooled blades for heavy-duty gas turbines. *Annals New York Academy of Sciences*, 934:179–193, 2001.

[5] C. Prakash and R. Zerkle. Prediction of turbulent flow and heat transfer in a radially rotating square duct. *Journal of Turbomachinery*, 114:835–846, 1992.

[6] A. K. Tolpadi. Calculation of heat transfer in a radially rotating coolant passage. *Numerical Heat Transfer, Part A*, 26:683–699, 1994.

[7] H. Iacovides, B. E. Launder, and H.-Y. Li. The computation of flow development through stationary and rotating u-ducts of strong curvature. *Int. J. Heat and Fluid Flow*, 17:22–33, 1996.

[8] T. Bo, H. Iacovides, and B. E. Launder. Developing buoyancy-modified turbulent flow in ducts rotating in orthogonal mode. *Journal of Turbomachinery*, 117:474–484, 1995.

[9] B. Bonhoff, U. Tomm, and B. V. Johnson. Heat transfer predictions for u-shaped coolant channels with skewed ribs and with smooth walls. *ASME Turbo Asia Conference, Jakarta, Indonesia*, 1996.

[10] B. Bonhoff, U. Tomm, B. V. Johnson, and I. Jennions. Heat transfer predictions for rotating u-shaped coolant channels with skewed ribs and with smooth walls. *ASME Gas Turbine & Aeroengine Congress & Exhibition, Orlando, Florida*, 1997.

[11] H.-C. Chen, Y.-J. Jang, and J.-C. Han. Computation of heat transfer in rotating two-pass square channels by a second-moment closure model. *International Journal of Heat and Mass Transfer*, 43:1603–1616, 2000.

[12] Y.-J. Jang, H.-C. Chen, and J.-C. Han. Flow and heat transfer in a rotating square channel with 45 deg angled ribs by reynolds stress turbulence model. *Journal of Turbomachinery*, 123:124–132, 2001.

[13] Y.-L. Lin, T. I.-P. Shih, M. A. Stephens, and M. K. Chyu. A numerical study of flow and heat transfer in a smooth and ribbed u-duct with and without rotation. *Journal of Heat Transfer*, 123:219–232, 2001.

[14] M. A. Stephens and T. I-P. Shih. Flow and heat transfer in a smooth u-duct with and without rotation. *Journal of Propulsion and Power*, 15:272–279, 1999.

[15] K.-S. P. Nikas and H. Iacovides. The computation of flow and heat transfer through an orthogonally rotating square-ended u-bend using low-reynolds-number models. *International Journal of Rotating Machinery*, 3:232–243, 2005.

[16] A. K. Saha and S. Acharya. Unsteady rans simulation of turbulent flow and heat transfer in ribbed coolant passages of different aspect ratios. *ASME Turbo Expo, Power for Land, Sea and Air, Vienna, Austria*, pages 1–13, 2004.

[17] A. K. Viswanathan and D. K. Tafti. Detached eddy simulation of turbulent flow and heat transfer in a two-pass internal cooling duct. *International Journal of Heat and Fluid Flow*, 27:1–20, 2005.

[18] A. Murata and S. Mochizuki. Effects of centrifugal buoyancy and reynolds number on turbulent heat transfer in a two-pass angled-rib-roughened channel with sharp 180° turns investigated by using large eddy simulation. *International Journal of Rotating Machinery*, 2008.

[19] F. M. White. *Viscous Fluid Flow*. McGraw-Hill, 3rd edition, 2006.

[20] ANSYS CFX Inc. *CFX 15.0 Modeling Guide*. ANSYS, Inc., Canonsburg, PA,USA, 2013.

[21] W. M. Kays and H. C. Perkins. *Handbook of Heat Transfer*, chapter Forced Convection, Internal Flow in Ducts. McGraw-Hill, 1973.

[22] P. J. Roache. Perspective: A method for uniform reporting of grid refinement studies. *Journal of Fluids Engineering*, 116:405–413, 1994.

[23] I. Celik and O. Karatekin. Numerical experiments on application of richardson extrapolation with nonuniform grids. *Journal of fluids engineering*, 119:584–590, 1997.

[24] F. R. Menter. Two-equation eddy-viscosity turbulence models for enginengine applications. *AIAA*, 32:1598–1605, 1994.

[25] P. E. Smirnov and F. R. Menter. Sensitization of the sst turbulence model to rotation and curvature by applying the spalart-shur correction term. *Journal of Turbomachinery*, 131:041010–1 – 041010–8, 2009.

[26] F. R. Menter, A. V. Garbaruk, and Y. Egorov. Explicit algebraic reynolds stress models for anisotropic wall-bounded flows. *EUCASS - 3rd European Conference for Aero-Space Sciences, Versailles, France*, 2009.

[27] J. H. Wagner, B. V. Johnson, and T. J. Hajek. Heat transfer in rotating passages with smooth walls and radial outward flow. *Journal of Turbomachinery*, 113:42–51, 1991.

[28] G. J. Hwang and T. C. Jen. Convective heat transfer in rotating isothermal ducts. *International Journal of Heat and Mass Transfer*, 33:1817–1828, 1990.